Sol-Gel Synthesis and Characterization of $Ba_{1-x}Gd_xTiO_{3+\delta}$ Thin Films on SiO₂/Si Substrates Using Spin-Coating Technique

Yen Chin TEH, Ala'eddin A. SAIF [*], Prabakaran POOPALAN

School of Microelectronic Engineering, University Malaysia Perlis (UniMAP), Pauh Putra Campus, 02600 Arau, Perlis, Malaysia

$Ba_{1-x}Gd_xTiO_{3+\delta}$, at x = 0, 0.05, 0.1, 0.15, 0.2, (BGT) thin films have been fabricated on SiO₂/Si substrate using sol-gel method. The microstructure and surface morphology of the fabricated films have been investigated using X-ray diffraction (XRD) and atomic force microscopy (AFM). The XRD results show that the fabricated films are crystalline with perovskite structure. There is a shifting of the preferred peak at 31.5° to a higher angle as the doping ratio increases suggesting a distortion lattice exists in the films, which could be due to the substitution of Gd^{3+} ions into Ba-site. The decreasing of lattice constants confirms the substitution of Gd^{3+} in BaTiO₃ lattice structure. The microstrain and dislocation density are found to be increased with the increase of Gd^{3+} doping, which attributed to the reduction of lattice volume that due to the ionic size mismatch effect. The AFM results show decreasing trend in both average grain size and roughness parameters. Therefore, the microstructure and surface morphology of BGT samples is strongly dependent on the Gd^{3+} doping concentration that mainly due to the difference ionic radius substitution.

Keywords: barium titanate, gadolinium doping, sol-gel, thin film, microstructure.

1. INTRODUCTION

Barium titanate (BaTiO₃) is a well-known ferroelectric material that has been widely used in many applications including microelectronic and optoelectronic devices due to its excellent dielectric constant and ferroelectric properties [1 – 3]. Due to its unique intrinsic capability of the perovskite structure that can host ions of different sizes, which allows many dopants to be accommodated in BaTiO₃ lattices [4]. Trivalent rare-earth ions are commonly used at low dopant levels in commercial formulations of BaTiO₃-based devices to improve its reliability on many properties [5]. Numerous experiments have been carried out to explore the incorporation effect of rare-earth dopants in BaTiO₃ properties. Among of them, gadolinium (Gd^{+3}) which possesses good optical properties and strong influences on electrical properties [6].

Few studies have investigated the effect of incorporation of Gd^{3+} dopant in barium titanate. Li et al. [7] have reported that Gd^{3+} ions substitution in Ba or Ti site within perovskite lattice depends on doping concentration, which affects directly on the dielectric constant of the final composite. Dale found that Gd^{3+} dopant has the greatest increment in the dielectric constant for barium titanate compared to other rare-earth dopant in his study [8]. However, the influence of Gd^{3+} on the microstructure lacks relevant research. It is essential to investigate the effect of Gd^{3+} doping in BaTiO₃ on microstructure and surface morphology as it affects many properties, including electrical and optical properties and gives many fundamental information such as friction, contact deformation, and electric conduction mechanism [9].

The microstructure and surface morphology of BaTiO₃ are strongly dependent on the synthesis process and fabrication methods. The traditional solid-state method has a strict criterion on particle size and purity of raw material, and required high operating temperature, which will acutely affect the product performance [1, 10]. Recently, the sol-gel method has been extensively attracted interest despite of its excellent control of stoichiometry, ease of compositional modifications and can produce homogeneous film deposition on large area substrates at relatively low annealing temperature using inexpensive equipment [11 – 15].

In this work, Gd-doped BaTiO₃ (BGT) thin films at different doping ratio will be prepared using sol-gel method. The microstructure of the prepared films will be deeply investigated via structural parameters. In addition, the grain size and surface roughness will be intensively studied using amplitude parameters.

2. EXPERIMENTAL DETAILS

BGT solutions at different molar ratios with the formula $Ba_{1-x}Gd_xTiO_{3+\delta}$ are prepared via sol-gel technique, where x = 0, 0.05, 0.1, 0.15, 0.2. Barium acetate, gadolinium acetate and titanium (IV) isopropoxide are used as starting materials together with glacial acetic acid and 2-methoxyethanol as solvent agents. Proportional amount of barium acetate and gadolinium acetate are dissolved in pre-heated glacial acetic at constant stirring for 1 hour, and then followed by refluxed at 120 °C for 1 hour to formed Ba:Gd solution. In a separate condition, titanium solution is prepared by drop-added a stoichiometric amount of titanium (IV) isopropoxide into 2-methoxyethanol and stirred at room temperature. Under constant stirring condition, the Ti solution is subsequently drip-added into Ba:Gd solution at room temperature. The mixture is later refluxed at 120 ºC

---

[*] Corresponding author. Tel.: +0142470306.
E-mail address: *alaeddinsaif@gmail.com* (A.A. Saif)

for 1 hour in order to obtain a transparent homogeneous solution. Lastly, the final solution is then filtered using a nylon syringe filter. Five solutions with different proportions of Ba:Gd, i.e. 1:0, 0.95:0.05, 0.90:0.10, 0.85:0.15, and 0.80:0.20, that are labelled as BGT0, BGT05, BGT10 BGT15, and BGT20, respectively, have been prepared.

Silicon substrates have been sequentially cleaned by following the standard cleaning process. A 15 nm of silicon dioxide has been thermally deposited on silicon substrates as buffer layer. The prepared solutions are spun-deposited on SiO_2/Si substrates using spin coater at speed of 4000 rpm for 20 seconds and then followed by post-heated at 200 °C for 20 minutes to vaporize organic solvents. Annealing process is then carried out on the as-deposited samples at 900 °C for 1 hour to form crystalline films. The phase analysis of BGT at various compositions is studied using X-ray diffractometer (XRD, D2 Phaser, Bruker) with Cu-K_α radiation source ($\lambda = 1.5406$ Å), scanning from 20° to 60° with a scan step of 0.02°, operated at a voltage of 30 kV and a current of 10 mA. XRD analysis gives information on size of the unit cell, lattice parameters and crystallite size accordingly. The lattice parameters, a and c, of the films can be determined using lattice geometry for tetragonal phase given by [16]

$$\frac{1}{d^2} = \frac{h^2 + k^2}{a^2} + \frac{l^2}{c^2},$$ (1)

where d is the interplanar spacing, and h, k and l are Miller indices. The average crystallite size of the BGT films can be calculated from the width at half height of the main diffraction peak (110) in Fig. 1 using Scherrer equation [17], which given by:

$$D = \frac{k\lambda}{\beta \cos\theta},$$ (2)

where D is the crystallite size, λ is the radiation wavelength of Cu-$k\alpha$, β is the full width at half maximum height of the peak (FWHM), $k = 0.9$ is the shape factor of the average crystallite and θ is the Bragg angle of the main diffraction peak. The dislocation density formula is given by [18]:

$$\delta_D = \left(\frac{5\xi}{D}\right)\left(\frac{h}{a} + \frac{k}{b} + \frac{l}{c}\right),$$ (3)

where ξ is the microstrain as $\xi = \beta \cos\theta/4$ and can be calculated using single XRD peak. The surface morphology analysis has been performed using Atomic Force Microscopy (AFM, SPA400, SII Nanotechnology, Inc) in contact mode. Area of 5 µm x 5 µm and 1 µm x 1 µm is scanned at four different positions on the sample surface away from the sample edges to avoid edge effect for surface roughness and average grain size, respectively. Specific roughness parameters have been extracted using Gwyddion software.

3. RESULTS AND DISCUSSION

The XRD patterns of Gd doped $BaTiO_3$ films annealed at 900 °C are illustrated in Fig. 1. It can be seen that the diffraction peaks for all films are (100), (110), (111), (200), and (211) within the 2θ range from 20° to 60°, which confirm that the films are crystallized with perovskite structure. It has been observed that the prepared substrate for this experiment show a high intensity peak at 22.5° that

match with the perovskite peak of (100), which explains the high intensity of the (100) diffraction peak in BGT samples. This peak is attributed to the crystalline structure of the SiO_2 grown in our lab. There are two peaks corresponding to secondary silicate phases (Fresnoite, $Ba_2TiSi_2O_8$) detected at 27.0° and 28.9°. These phases could be attributed to the incorporation of a small amount of BGT with the substrate which due the diffusion of silicon into BGT films arise very fast at high-temperature heating process and formed interfacial silicate [19]. However, the formation of Fresnoite peak can be avoided by growing a thicker layer of buffer layer [20].

On the other hand, a decrease of diffraction intensity for the orientations (110), (111), (200) and (211) planes is observed as Gd^{3+} ratio concentration increases. This decrement of diffraction intensity is due to the distortion of lattice arrangement in the perovskite lattice due to the substitution of Gd^{3+} into Ba^{2+} sites. Generally, the diffraction intensities reflect the total scattering from $BaTiO_3$ crystal structure, and are directly proportional to the concentration of the compound that exhibit it [21, 22]. In other words, the concentration of Ba^{2+} reduces as the Gd^{3+} increases and results in lower diffraction intensity. Besides that, it is observed that the peaks getting broader as Gd concentration increases, which is more obvious for the main diffraction peak of (110).
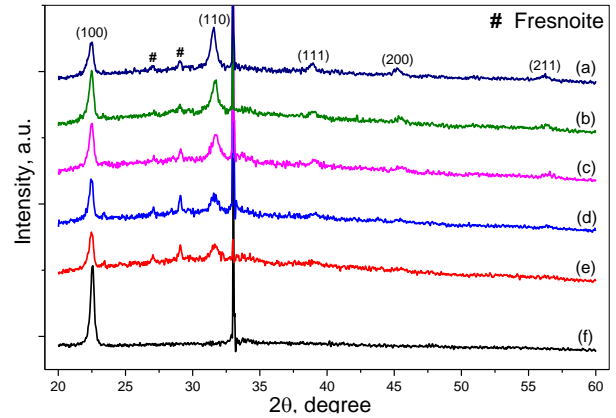
Fig. 1. XRD patterns at different Gd doping ratio of: a – BGT0; b – BGT05; c – BGT10; d – BGT15; e – BGT20; f – substrate

This broadening increment could be attributed to the changes of crystallite size in the films. The calculated crystallite size is tabulated in Table 1, which shows that the crystallite size of BGT reduces from 21.041 nm to 11.269 nm as the Gd^{3+} doping increases.

From XRD results, it is observed that the main diffraction peak at 31.4° for the samples that are doped with Gd^{3+} shifts toward a higher angle. This could be explained based on ionic substitution mechanism within the lattice. Gd^{3+} ion has intermediate ionic radius of 0.094 nm compared to Ba^{2+} and Ti^{4+} ions, therefore, the substitution of Gd^{3+} into Ba/Ti site will result in shrink/expand of the lattice, and the diffraction peak will either shift toward a higher degree or a lower degree [23]. The shifting toward higher angle in this case indicates that Gd^{3+} ions occupies Ba^{2+} sites, and it is in good agreement with Gama's result [24].

Dislocation is a crystallographic deformity within a crystal structure and it strongly influences number of

physical properties of the material [25]. The calculated lattice parameters, microstrain and dislocation density are tabulated in Table 1. It is found that both *a* and *c* lattice constants are slightly reduced and a gradual contraction of the lattice volume is observed as the Gd^{3+} doping ratio increases. Tsur et al. [26] found that lattice shrinks with the substitution of ionic rare earth on Ba-site and expanded with ionic rare-earth on the Ti-site. Ben and Sinclair [27] found that replacement of smaller doping ion in Ba-site results in decrease in lattice volume as the doping ratio increased. Accordingly, the decreasing in lattice volume confirmed the substitution of Gd^{3+} in Ba-site [28].

On the contrary, both microstrain and dislocation density are found to be increased with the increase of Gd^{3+} doping ratio. This increment is attributed to the ionic size mismatch effect on the A-site between Ba^{2+} and Gd^{3+} ions [27]. The substitution of Gd^{3+} in perovskite lattice causes distortion in the size of the lattice unit and reduces its volume as discussed earlier. The reduction in the lattice volume results in lattice mismatch and consequently, creates more vacancies between grains, which contributes to a larger area in grain boundaries [29] and leads to higher microstrain and dislocation density with the increase of Gd^{3+} doping ratio. Generally, the current thin films show relatively low dislocation density values compared to bulk form [24].

AFM analysis is carried out to investigate the surface morphology in terms of grain size and roughness on different doping ratio of BGT deposited on SiO$_2$/Si substrates. Fig. 2 shows two-dimensional AFM micrographs of one layer samples at different doping concentrations of Gd^{3+}. It can be seen from BT sample in Fig. 2 a that the grains are agglomerated and evenly distributed over the scanned area. As the Gd^{3+} ions are introduced into BT, the grains obviously become smaller in size and formed in clusters distributed uniformly over the surface as shown in Fig. 2 e. It is clearly seen that the bright grains in the AFM micrographs in Fig. 2 represent the grains closer to detector.

The average grain size of these samples has been measured in diameter and is plotted as a function of Gd^{3+} doping concentration which illustrated in Fig. 3. The diameter of each grain is measured at different points and the average value is taken to ensure the accuracy of the measured grain size. The graph shows a decrement trend of grain size from 158.74 nm to 62.87 nm as the Gd^{3+} doping concentration increased, which is in agreement with Li's results [7]. The grain size decrement can be attributed to inhibition behaviour of the grains due to Gd^{3+} ions substitution at Ba^{2+} in perovskite lattice. It is interesting to mention here that the decreasing trend of the measured grain size is agreed with the calculated crystallite size from XRD results. However, it is well known that the grain might contain several crystallites which explain the large value of the grain size compared to the crystallite size for the same ratio of doping. The inhibition of grain growth is similar with Pal's result [30], thus it is confirmed that Gd^{3+} act as a grain growth inhibitor.

Fig. 4 shows three-dimensional micrographs of single layer samples at different doping ratio of Gd^{3+}. From the micrographs, it can be seen that fine and sharp peaks are well-distributed over the scanned area indicating that the surface of fabricated films are dense and smooth with crack-free. The surface morphology of the tested samples is quantitatively evaluated using amplitude analysis [9]. The average roughness of the films has been extracted and plotted as a function of Gd^{3+} ratio which shown in Fig. 5. The relatively low value of R$_a$ indicates the fabricated BGT film surfaces are smooth. From Fig. 5, the average roughness is almost linearly decreases as the Gd doping ratio increases.

This decreasing trend is due to the grain growth inhibition mechanism over the scanned area. The decreasing of R_a also can be mathematically explained through equation given by [9]:

$$R_a = \frac{1}{L} \int_0^L |y(x)| . dx , \qquad (4)$$

where *L* is the length of the profile on the x-axis used for measurement and *y(x)* is the variation of the height from the profile line for each data point.

Table 1. Distinct structural parameters of BGT at different doping concentration of Gd

Sample	FWHM, degree	Crystallite size, nm	Lattice constant, Å		Lattice volume, Å^3	Microstrain η, (x10^{-3})	Dislocation density δ_D, µm^{-2}
			a	*c*			
BGT0	0.443	21.041	4.000	4.056	64.877	1.647	1863.46
BGT05	0.489	19.087	3.987	4.049	64.365	1.816	2386.35
BGT10	0.579	16.128	3.985	4.024	63.908	2.149	3344.02
BGT15	0.717	13.008	3.982	4.008	63.538	2.665	5145.12
BGT20	0.828	11.269	3.975	4.014	63.442	3.076	6866.84
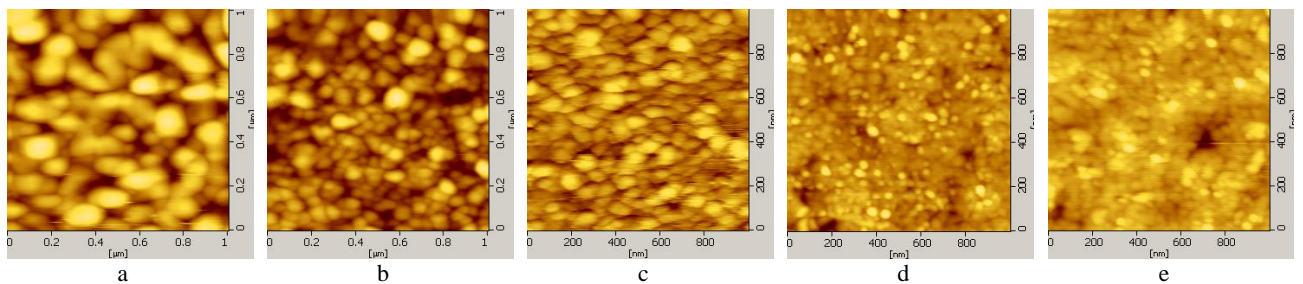
Fig. 2. Two-dimensional AFM micrograph at different Gd doping ratio: a – BGT0; b – BGT05; c – BGT10; d – BGT15; e – BGT20

The profile height represents each grain on the surface, as the grain size reduces, the number of profile height associated to the grain increases over the same scan area leading to roughness decreases. The others of amplitude parameters are summarized in Table 2.
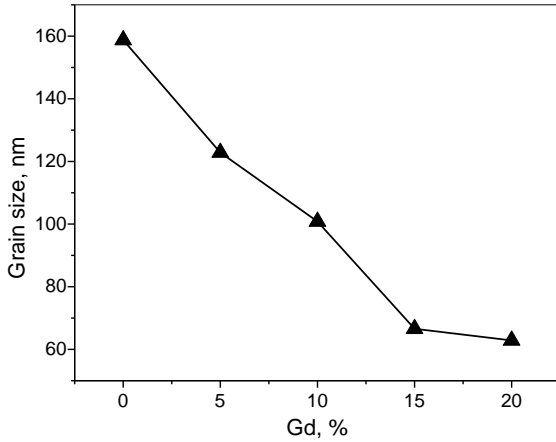

Fig. 3. Grain size of one layer sample at variation Gd doping ratio

From Table 2, both parameters of RMS roughness (R_q) values and maximum peak to valley height roughness (R_t) values show the same trend as the average roughness values for different doping concentrations which also can be mathematically explained according to given formulas [9]:

$$R_q = \sqrt{\frac{1}{L} \int_0^L \left| (y(x))^2 \right| . dx}, \tag{5}$$

$$R_t = \frac{1}{n} \left(\sum_{i=1}^n P_i - \sum_{i=1}^n V_i \right), \tag{6}$$

where n is the number of sampling points along the assessment length, which is 5 in this study, P_i is the height of the i-th peak and V_i is the depth of the i-th valley with respect to the line profile. However, R_t for BGT05 in this case is lack of this trend which believed due to large distance of maximum peak to valley as seen in Fig. 4 b. The positive sign of skewness roughness (R_{sk}) values indicates the samples surface is predominant with peaks [31]. For roughness kurtosis, BGT 05 and BGT 10 show value greater than three which revealed a spiky surface. On the other hand, samples with R_{sk} value lower than three demonstrated a bumpy surface. The formation of spiky surface and bumpy surface is probably attributed to the sample preparation processes.
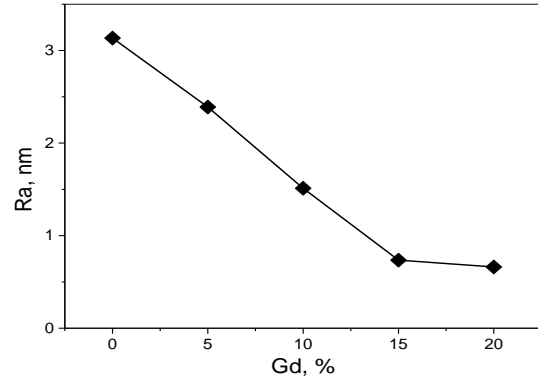
Fig. 5. Average roughness of the tested samples as a function of variation Gd^{3+} doping concentration

Table 2. The amplitude parameters of tested samples at different Gd doping ratio

Sample	R_a, nm	R_q, nm	R_t, nm	R_{sk}, nm	R_{ku}, nm
BT	3.134 ±0.112	3.930 ±0.137	39.670 ±0.851	0.304 ±0.035	0.191 ±0.033
BGT05	2.389 ±0.066	3.495 ±0.212	48.708 ±0.976	2.008 ±0.017	8.793 ±0.176
BGT10	1.512 ±0.012	2.037 ±0.022	40.970 ±3.514	0.729 ±0.035	13.470 ±0.622
BGT15	0.736 ±0.095	0.950 ±0.108	10.493 ±0.819	0.915 ±0.018	0.964 ±0.008
BGT20	0.662 ±0.029	0.860 ±0.036	9.371 ±0.994	0.852 ±0.029	1.668 ±0.014

a

b

c

d

e
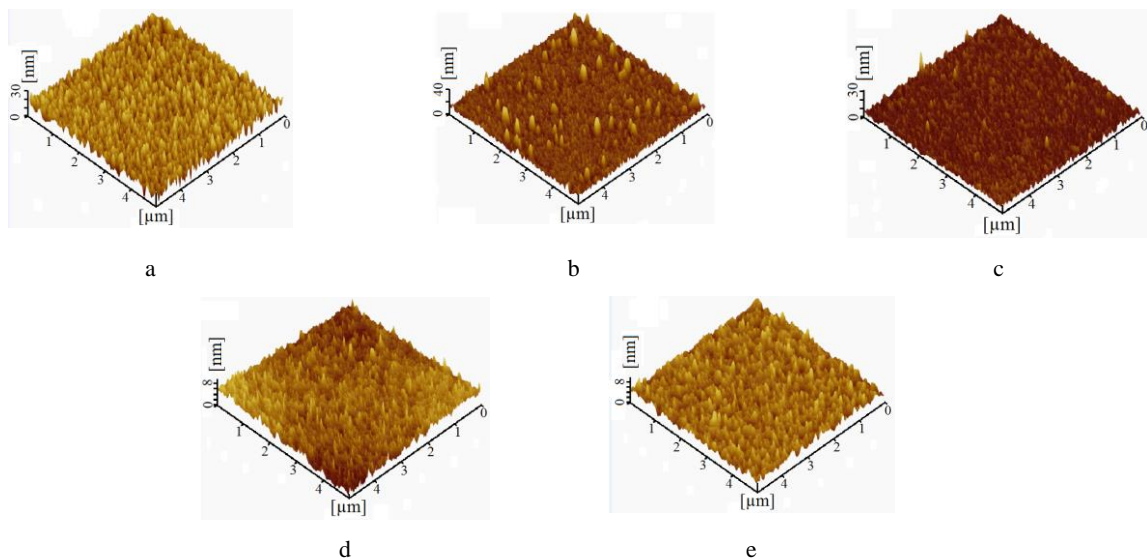
Fig. 4. Three-dimensional AFM micrographs at different Gd doping ratio: a – BT; b – BGT05; c – BGT10; d – BGT15; e – BGT20

4. CONCLUSIONS

Gadolinium doped barium titanate ($Ba_{1-x}Gd_xTiO_{3+\delta}$) thin films have been successfully fabricated on SiO_2/Si substrate using spin coating method. The microstructure and surface morphology of the fabricated films have been characterized using XRD and AFM. The diffraction peaks in XRD results reveal that the samples are crystallized with perovskite structure. A small peak corresponding to secondary silicate phases is detected at 27.0º and 28.9º, which is due to the diffusion of Si into $BaTiO_3$. There is a small shift for the main diffraction peak of the samples that are doped with Gd^{3+} ions towards a higher degree, suggested that the Gd^{3+} ions have substituted into Ba-site in the perovskite structure. The crystallite size is calculated using Scherrer equation, which shows a decrement from 21.041 nm to 11.269 nm as Gd^{3+} doping ratio increases confirming that Gd^{3+} ions have replaced Ba-sites and leads to a reduction in lattice volume. The dislocation density in the films increased from 1863.46 μm^{-2} to 6866.84 μm^{-2} with the Gd^{3+} doping ratio. This increment is due to the ionic size mismatch effect, which contributes to larger grain boundaries area and higher microstrain and dislocation density.

From AFM results, the average grain size of all samples decreases from 158.74 nm to 62.87 nm with the increase of Gd^{3+} doping ratio, which is attributed to the reduction lattice due to substitution of Gd^{3+} in Ba-site, that is in line with XRD results. Same trend is noticed for surface roughness, R_a, of the samples which can be explained through the reduction of grain size over the scanned area. The skewness roughness values show that the tested films' surfaces are uniformly distributed with peak as dominant. Nevertheless, kurtosis roughness values reveal both spiky and bumpy surfaces, which are believed due to the fabrication processes. Therefore, it can be concluded that the microstructure and surface morphology of BGT samples is strongly dependent on the Gd^{3+} doping concentration and is mainly due to the difference ionic radius substitution

REFERENCES

1. **Li, W., Xu, Z., Chu, R., Fu, P., Hao, J.** Structure and Electrical Properties of $BaTiO_3$ Prepared by Sol Gel Process *Journal Alloys Compound* 482 2009: pp. 137 – 140. http:// dx.doi.org:10.1016/j.jallcom.2009.02.137

2. **Cernea, M.** Methods for Preparation of $BaTiO_3$ Thin Films *Journal of Opotoelectronics Advanced Materials* 6 (4) 2004: pp. 1349 – 1356.

3. **Pontes, F.M., Pinheiro, C.D., Longo, E., Leite, E.R., de Lazaro, S.R., Magnani, R., Pizani, P.S., Boschi, T.M., Lanciotti, F.** Theoretical and Experimental Study on the Photoluminescence in $BaTiO_3$ Amorphous Thin Films prepared by the chemical route *Journal of Luminescence* 104 2003: pp. 175 – 185. http://dx.doi.org:10.1016/S0022-2313(03)00014-0

4. **Buscaglia, M.T., Buscaglia, V., Viviani, M., Nanni, P., Hanuskova, M.** Influence of Foreign Ions on the Crystal Structure of $BaTiO_3$ *Journal of the European Ceramic Society* 20 2000: pp. 1997 – 2007. http://dx.doi.org:10.1016/S0955-2219(00)00076-5

5. **Kishi, H., Mizuno, Y., Chazono, H.** Base-Metal Electrode-Multilayer Ceramic Capacitors: Past, Present and Future Perspectives *Japanese Journal of Applied Physics* 42 (1) 2003: pp. 1 – 15. http://dx.doi.org/10.1143/JJAP.42.1

6. **Fasasi, A.Y., Ngom, B.D., Kana-Kana, J.B., Bucher, R., Maaza, M., Theron, C., Butther, U.** Synthesis and Characterisation of Gd-doped $BaTiO_3$ Thin Films Prepared by Laser Ablation for Optoelectronic Applications *Journal of Physics and Chemistry of Solids* 70 2009: pp. 1322 – 1329. http://dx.doi.org:10.1016/j.jpcs.2009.06.022

7. **Li, L., Wang, M., Guo, D., Fu, R., Meng, Q.** Effect of Gd Amphoteric Substitution on Structure and Dielectric Properties of BaTiO3-Based Ceramics *Journal of Electroceramics* 30 2013: pp. 129 – 132. http://dx.doi.org:10.1007/s10832-012-9773-9

8. **Dale, G., McLaughlin, J., Conway, M.** An Investigation into the Electrical Properties of Doped BaRium Titanate using EIS *Applications of Ferroelectrics held jointly with 2012 European Conference on the Applications of Polar Dielectrics and 2012 International Symp Piezoresponse Force Microscopy and Nanoscale Phenomena in Polar Materials (ISAF/ECAPD/PFM)* 2012: pp. 1 – 3. http://dx.doi.org:10.1109/ISAF.2012.6297809

9. **Gadelmawla, E.S., Koura, M.M., Maksoud, T.M.A., Elewa, I.M., Soliman, H.H.** Roughness Parameters *Journal of Materials Processing Technology* 123 2002: pp. 133 – 145. http://dx.doi.org: 10.1016/S0924-0136(02)00060-2

10. **Aitasalo, T., Hölsa, J., Jungner, H., Lastusaari, M., Niittykoski, J.** Comparison of Sol-Gel and Solid State Prepared Eu2+ Doped Calcium Aluminates *Materials Science* 20 (1) 2002: pp. 15 – 20.

11. **Sedlar, M., Sayer, M., Weaver, L.** Sol-Gel Processing and Properties of Cerium Doped Barium Strontium Titanate Thin Films *Journal of Sol-Gel Science and Technology* 5 1995: pp. 201 – 210. http://dx.doi.org: 10.1007/BF00487017

12. **Yu, Y.J., Chan, H.L.W., Wang, F.P., Li, K., Choy, C.L., Zhao, L.C.** Structural and Ferroelectric properties of Europium Doped Lead Zirconate Titanate Thin Films by a Sol-Gel Method *Thin Solid Films* 424 2003: pp. 161 – 164. http://dx.doi.org: 10.1016/S0040-6090(02)01052-0

13. **Ramesh, J., Pasupathi, G., Mariappan, R., Senthil Kumar, V., Ponnuswamy, V.** Structural and Optical Properties of Ni Doped ZnO Thin Films using Sol-Gel Dip Coating Technique *Optik* 124 2013: pp. 2023 – 2027. http://dx.doi.org: 10.1016/j.ijleo.2012.06.035

14. **Sakka, S.** Sol-Gel Coating Films for Optical and Electronic Application. Springer, Berlin, 1996: pp. 1 – 49.

15. **Xu, Y.** Ferroelectric Thin Films Fabricated by Sol-Gel Technique *Proceedings 6th International Conference on Solid State and Integrated-Circuit Technology* 2001: pp. 696 – 701. http://dx.doi.org: 10.1109/ICSICT.2001.981599

16. **Pakizeh, E., Moradi, M., Ahmadi, A.** Effect of Sol-Gel pH on XRD Peak Broadening , Lattice Strain, Ferroelectric Domain Orientation, and Optical Bandgap of Nanocrystalline $Pb_{1.1}(Zr_{0.52}Ti_{0.48})O_3$ *Journal of Physics and Chemistry of Solids* 75 2014: pp. 174 – 181.

17. **Monshi, A., Foroughi, M.R., Monshi, M.R.** Modified Scherrer Equation to Estimate More Accurately Nano-Crystalline Size using XRD *World Journal of Nano Science and Engineering* 2 2012: pp. 154 – 160.

http://dx.doi.org: 10.4236/wjnse.2012.23020

18. **Reddy, N.K., Ramesh, K., Ganesan, R., Reddy, K.T.R., Gunasekhar, K.R., Gopal, E.S.R.** Synthesis and Characterisation of Co-Evaporated Tin Sulphide Thin Films *Applied Physics A: Materials Science and Processing* 83 2006: pp. 133 – 138.
http://dx.doi.org: 10.1007/s00339-005-3475-y

19. **Stawski, T.M., Vijselaar, W.J.C., Göbel, O.F., Veldhuis, S.A., Smith, B.F., Blank, D.H.A., Elshof, J.E.T.** Influence of High Temperature Processing of Sol-Gel Derived Barium Titanate Thin Films Deposited on Platinum and Strontium Ruthenate Coated Silicon Wafers *Thin Solid Films* 520 2012: pp. 4394 – 4401.
http://dx.doi.org: 10.1016/j.tsf.2012.02.029

20. **George, J.P., Beeckman, J., Woestenborghs, W., Smet, P.F., Bogaerts, W., Neyts, K.** Preferentially Oriented $BaTiO_3$ Thin Films Deposited on Silicon with Thin Intermediate Buffer Layers *Nanoscale Research Letters* 8 (62) 2013: pp. 1 – 7.
http://dx.doi.org: 10.1186/1556-276X-8-62

21. **Norrish, K., Taylor, R.M.** Quantitative Analysis by X-ray Diffraction *Clay Minerals* 1962: pp. 98 – 109.

22. **Connolly, J.R.** Introduction Quantitative X-ray Diffraction Methods 2012: pp. 1 – 15.

23. **Kishi, H., Kohzu, N., Sugino, J., Ohsato, H., Iguchi, Y., Okuda, T.** The Effect of Rare-earth (La, Sm, Dy, Ho and Er) and Mg on the Microstructure in $BaTiO_3$ *Journal of the European Ceramic Society* 19 1999: pp. 1043 – 1046.
http://dx.doi.org: 10.1016/S0955-2219(98)00370-7

24. **Gama, S.B., Raibagkar, R.L.** Influence of Sintering Aids on Structural Characteristics of $(Ba_{1-x}Gd_x)TiO_3$ *World Research Journal of Applied Physics* 1 (1) 2010: pp. 5 – 13.
http://dx.doi.org: 10.1016/j.jpcs.2013.09.005

25. **Borah, M., Mohanta, D.** Effect of Gd3+ Doping on Structural, Optical and Frequency-Dependent Dielectric Response Properties of Pseudo-Cubic $BaTiO_3$ Nanostructures *Applied Physics A: Materials Science and Processing* 115 2013: pp. 1057 – 1067.
http://dx.doi.org: 10.1007/s00339-013-7941-7

26. **Tsur, Y., Dunbar, T.D., Randall, C.A.** Crystal and Defect Chemistry of Rare Earth Cations in $BaTiO_3$ *Journal of Electroceramics* 7 2001: pp. 25 – 34.
http://dx.doi.org: 10.1023/A:1012218826733

27. **Ben, L., Sinclair, D.C.** Anomalous Curie Temperature Behavior of A-Site Gd-Doped BaTiO3 Ceramics: The Influence of Strain *Applied Physics Letters* 98 2011: pp. 092907 1 – 3.
http://dx.doi.org/10.1063/1.3563710

28. **Jiang, W., Cai, W., Lin, Z., Fu, C.** Effects of Nd-Doping on Optical and Photovoltaic Properties of Barium Titanate Thin Films Prepared by Sol-Gel Method *Materials Research Bulletin* 48 2013: pp. 3092 – 3097.
http://dx.doi.org: 10.1016/j.materresbull.2013.04.048

29. **Saif, A.A., Poopalan, P.** Correlation between the Chemical Composition and the Conduction Mechanism of Barium Strontium Titanate Thin Films *Journal of Alloys and Compounds* 509 2011: pp. 7210 – 7215.
http://dx.doi.org: 10.1016/j.jallcom.2011.04.068

30. **Pal, V., Dwivedi, R.K., Thakur, O.P.** Synthesis and ferroelectric behavior of Gd Doped BNT Ceramics *Current Applied Physics* 14 2014: pp. 99 – 107.
http://dx.doi.org: 10.1016/j.cap.2013.10.007

31. **Teh, Y.C., Saif, A.A., Jamal, Z.A.Z., Poopalan, P.** Microstructure Study on Gd-doped BaTiO3 Sol-gel Multilayer Thin Films using AFM for Optoelectronic Applications *Advanced Materials Research* 911 2014: pp. 251 – 255.
http://doi:10.4028/www.scientific.net/AMR.911.251